

Role of Cell Surface Lipopolysaccharides in *Escherichia coli* K12 Adhesion and Transport

Sharon L. Walker, Jeremy A. Redman, and Menachem Elimelech*

Department of Chemical Engineering, Environmental Engineering Program,
Yale University, P.O. Box 208286, New Haven, Connecticut 06520-8286

Received February 25, 2004. In Final Form: June 2, 2004

The influence of bacterial surface lipopolysaccharides (LPS) on cell transport and adhesion has been examined by use of three mutants of *Escherichia coli* K12 with well-characterized LPS of different lengths and molecular composition. Two experimental techniques, a packed-bed column and a radial stagnation point flow system, were employed to investigate bacterial adhesion kinetics onto quartz surfaces over a wide range of solution ionic strengths. Although the two systems capture distinct deposition (adhesion) mechanisms because of their different hydrodynamics, similar deposition kinetics trends were observed for each bacterial strain. Bacterial deposition rates were directly related to the electrostatic double layer interaction between the bacteria and quartz surfaces, in qualitative agreement with classic Derjaguin–Landau–Verwey–Overbeek (DLVO) theory. However, DLVO theory does not fully explain the deposition behavior for the bacterial strain with the lengthy, uncharged O-antigen portion of the LPS. Neither the length nor the charge characteristics of the LPS molecule directly correlated to deposition kinetics, suggesting a complex combination of cell surface charge heterogeneity and LPS composition controls the bacterial adhesive characteristics. It is further suggested that bacterial deposition behavior is determined by the combined influence of DLVO interactions, LPS-associated chemical interactions, and the hydrodynamics of the deposition system.

1. Introduction

The fundamental mechanisms involved in bacterial attachment to surfaces are of paramount importance in diverse fields of engineering and science. Understanding the initial rate of bacterial adhesion can provide insights into the early stages of infection,^{1–3} biofilm formation on solid surfaces,⁴ and pathogen transport in subsurface environments.⁵ Due to the considerable importance of bacterial adhesion, the interaction forces surmised to govern cell attachment—classic DLVO-type forces⁶ and, in some cases, hydrophobic interactions^{7,8}—have been studied extensively.

Previous studies have also attributed the adhesive nature of bacteria to various cell surface features, such as outer membrane proteins,⁹ fimbriae,^{10,11} flagella,¹² and extracellular polymeric substances (EPS).^{13,14} These surface macromolecules have been characterized extensively

and their adhesive properties have been found to be sensitive to solution chemistry and environmental stresses.¹⁵ It has also been well documented that bacterial surface molecules facilitate the development of biofilms on medical implants, contact lenses, and teeth.^{1,16–18} One additional important surface molecule, the lipopolysaccharide (LPS), has also been implicated in playing a role in cell interaction with surfaces.^{19–21} This molecule is of considerable interest for the study of bacterial adhesion and transport, as it is ubiquitous on all Gram-negative bacteria, which comprise the majority of culturable cells found in aquatic environments.²²

Approximately 3.5 million LPS molecules are present on the outer membrane of Gram-negative bacteria, with significant variations in LPS coverage density and local distribution.^{23,24} The LPS is anchored to the lipid bilayer membrane by a lipid moiety known as lipid A.²⁵ Lipid A has been studied in the past due to its involvement in pathogenesis once the bacterium has adhered to a host

* Corresponding author: phone (203) 432-2789; fax (203) 432-2881; e-mail menachem.elimelech@yale.edu.

(1) Razatos, A.; Ong, Y. L.; Sharma, M. M.; Georgiou, G. *J. Biomater. Sci.—Polym. Ed.* **1998**, *9*, 1361.
(2) Mohamed, N.; Teeters, M. A.; Patti, J. M.; Hook, M.; Ross, J. M. *Infect. Immun.* **1999**, *67*, 589.
(3) Lamba, N. M. K.; Baumgartner, J. N.; Cooper, S. L. *J. Biomater. Sci.—Polym. Ed.* **2000**, *11*, 1227.
(4) Espinosa-Urgel, M.; Salido, A.; Ramos, J. L. *J. Bacteriol.* **2000**, *182*, 2363.
(5) Ginn, T. R.; Wood, B. D.; Nelson, K. E.; Scheibe, T. D.; Murphy, E. M.; Clement, T. P. *Adv. Water Resour.* **2002**, *25*, 1017.
(6) Derjaguin, B. V.; Landau, L. *Acta Physicochim. U.S.S.R.* **1941**, *14*, 300.
(7) Azeredo, J.; Visser, J.; Oliveira, R. *Colloid Surf. B—Biointerfaces* **1999**, *14*, 141.
(8) Ong, Y. L.; Razatos, A.; Georgiou, G.; Sharma, M. M. *Langmuir* **1999**, *15*, 2719.
(9) Navarre, W. W.; Schneewind, O. *Microbiol. Mol. Biol. Rev.* **1999**, *63*, 174.
(10) Soto, G. E.; Hultgren, S. J. *J. Bacteriol.* **1999**, *181*, 1059.
(11) Otto, J.; Norbeck, J.; Larsson, T.; Karlsson, K. A.; Hermansson, M. *J. Bacteriol.* **2001**, *183*, 2445.
(12) Prigent-Combaret, C.; Prensier, G.; Le Thi, T. T.; Vidal, O.; Lejeune, P.; Dorel, C. *Environ. Microbiol.* **2000**, *2*, 450.
(13) Frank, B. P.; Belfort, G. *J. Membr. Sci.* **2003**, *212*, 205.

(14) Tsuneda, S.; Aikawa, H.; Hayashi, H.; Yuasa, A.; Hirata, A. *FEMS Microbiol. Lett.* **2003**, *223*, 287.
(15) Poortinga, A. T.; Bos, R.; Norde, W.; Busscher, H. J. *Surf. Sci. Rep.* **2002**, *47*, 3.
(16) Greene, C.; McDevitt, D.; Francois, P.; Vaudaux, P. E.; Lew, D. P.; Foster, T. J. *Mol. Microbiol.* **1995**, *17*, 1143.
(17) Garcia-Saenz, M. C.; Arias-Puente, A.; Fresnadillo-Martinez, M. J.; Matilla-Rodriguez, A. *J. Cataract. Refract. Surg.* **2000**, *26*, 1673.
(18) Bruinsma, G. M.; Rustema-Abbing, M.; van der Mei, H. C.; Busscher, H. J. *J. Microbiol. Methods* **2001**, *45*, 95.
(19) Flemming, C. A.; Palmer, R. J.; Arrage, A. A.; Van der Mei, H. C.; White, D. C. *Biofouling* **1999**, *13*, 213.
(20) Abu-Lail, N. I.; Camesano, T. A. *Environ. Sci. Technol.* **2003**, *37*, 2173.
(21) Kannenberg, E. L.; Carlson, R. W. *Mol. Microbiol.* **2001**, *39*, 379.
(22) Fletcher, M. In *Bacterial Adhesion Molecular and Ecological Diversity*; Fletcher, M., Ed.; John Wiley and Sons: New York, 1996.
(23) Kotra, L. P.; Golemi, D.; Amro, N. A.; Liu, G. Y.; Mobashery, S. *J. Chem. Soc.* **1999**, *121*, 8707.
(24) Rietschel, E. T.; Kirikae, T.; Schade, F. U.; Mamat, U.; Schmidt, G.; Loppnow, H.; Ulmer, A. J.; Zahring, U.; Seydel, U.; Dipadova, F.; Schreier, M.; Brade, H. *FASEB J.* **1994**, *8*, 217.
(25) Madigan, M. T.; Martinko, J. M.; Parker, J. *Brock Biology of Microorganisms*, 8th ed.; Prentice Hall: Upper Saddle River, NJ, 1997.

cell, and it is often referred to as an endotoxin.²⁵ Directly bound to lipid A is 3-deoxy-D-manno-octulosonic (or 2-keto-3-deoxyoctonic) acid (KDO),^{25,26} which is an imperative part of the LPS structure, as it imparts viability to the cell by linking the core portion of the LPS to lipid A.^{27,28}

Early work designated an "inner" core of the LPS as the region containing heptoses and KDO, and an "outer" core as the region containing hexose and hexosamine groups.²⁷ In this paper we use newer terminology, designating the core polysaccharide region of the LPS as the portion immediately linked to the lipid A molecule, consisting of the KDO, heptoses (seven-carbon sugar groups), glucose, galactose, and *N*-acetylglucosamine.^{25,27} Gram-negative cells with LPS terminating after the core polysaccharide are often referred to as "rough" mutants.²⁷ The outermost portion of the LPS assembly linked to the core polysaccharide region is the O-antigen, also referred to as the O-specific chain. The exact size and composition of this polysaccharide is strain-specific.²¹ The O-antigen is generally composed of six-carbon sugar groups in repeating units consisting of four or five sugar sequences with a branched or linear geometry.²⁵ For *Escherichia coli*, the bacterium investigated in this paper, the number of repeated units can range from zero up to 40.²³ It has been reported that this lengthy portion of the LPS molecule can extend distances greater than 30 nm into the surrounding medium.^{28,29}

Systematic studies addressing the role of LPS in cell adhesion and transport are rather scarce. Such studies were limited to filtration experiments in packed-bed columns,^{29,30} where hydrodynamic flow conditions are not well-defined and microscopic observation of bacterial transport and adhesion is not possible. Other studies attempting to understand the role of LPS utilized atomic force microscopy (AFM) to image cells and to measure the interaction forces between an AFM tip and a bacterium surface.^{1,8,20,31,32} While AFM can provide useful information on the interaction forces involved, it does not allow the investigation of the role of hydrodynamics and the possible interrelationship between LPS-related interactions and hydrodynamic forces. To better understand the role of LPS in bacterial adhesion under flow conditions, it is necessary to use systems with well-characterized hydrodynamics, such that mechanisms of bacterial adhesion can be elucidated at the microscopic scale. Furthermore, to test the applicability of classic Derjaguin–Landau–Verwey–Overbeek (DLVO) theory to describe bacterial adhesion, it is imperative that relatively simple solution chemistries be employed.

The objective of this paper is to examine the role of LPS in the initial stages of bacterial adhesion under well-controlled solution chemistry and hydrodynamic conditions. Three *E. coli* K12 mutants having well-characterized LPS molecules of different lengths were selected to allow a systematic investigation of the role of LPS in cell adhesion. Two experimental techniques, a packed-bed column and a radial stagnation point flow (RSPF) system, were employed to study bacterial adhesion kinetics at both

the macroscopic and microscopic levels. Bacterial adhesion rates obtained from these two experimental systems over a wide range of ionic strengths were used to elucidate the role of LPS and the mechanisms governing bacterial adhesion under dynamic flow conditions.

2. Materials and Methods

2.1. Bacterial Cell Selection and Preparation. Mutants of the *E. coli* K12 strain, D21 and D21f2, used in this study were obtained from the *E. coli* Genetic Stock Center at Yale University. An additional *E. coli* K12 strain, JM109, was obtained from New England Biolabs (Beverly, MA). The K12 strain is very well-characterized, allowing for the selection of specific mutants based on the presence of distinct portions of the LPS molecule.³³ The parent strain D21 produces the core portion of the LPS molecule, while D21f2 is an isogenic mutant of D21 with a truncated LPS molecule.³⁴ JM109 has been reported as expressing a full core portion of the LPS as well as the extended O-antigen polysaccharide chain.²⁹

To visualize the cells in the radial stagnation point flow (RSPF) system, a plasmid coding for an enhanced green-fluorescing protein and gentamicin resistance³⁵ was introduced to the native D21, D21f2, and JM109 cells via electroporation following standard protocols.³⁶ The resulting transformed cell lines are referred to as D21g, D21f2g, and JM109g, respectively.

Cells were incubated in Luria–Bertani broth at 37 °C (LB broth; Fisher, Fair Lawn, NJ) in the presence of 0.03 mg/L gentamicin (Sigma, St. Louis, MO) for 3 h, after which they were harvested for use in experiments. The bacterial suspension was centrifuged (Sorvall RC26 Plus) for 15 min at 3823g in an SS34 rotor (Kendro Laboratory Products, Newtown, CT) to separate whole cells from the growth medium. The medium was decanted and the pellet was resuspended in a 10⁻² M KCl solution. To ensure all traces of growth medium were removed, the process of centrifuging, decanting, and resuspending in the electrolyte solution was repeated twice. The electrolyte solution used during this rinsing process was prepared with deionized water (Barnstead Thermolyne Corp., Dubuque, IA) and reagent-grade KCl (Fisher) with no pH adjustment (pH 5.6–5.8).

2.2. Bacterial Cell Characterization. The electrophoretic mobility of the bacterial cells was measured at 25 °C (ZetaPals, Brookhaven Instruments Corp, Holtsville, NY). An aliquot of the freshly harvested bacteria was suspended in a background KCl solution (10⁵–10⁶ cells/mL) and used for electrophoretic mobility measurement immediately prior to experimentation in the packed-bed column. The electrophoretic mobility was measured at least twice at each ionic strength. Zeta potentials were calculated from the measured electrophoretic mobilities by use of the tabulated numerical values in Ottewill and Shaw,³⁷ which accounts for retardation and relaxation effects.

To determine the average bacterial size, images of the three *E. coli* strains suspended in an electrolyte solution (approximately 10⁷ cells/mL in 10 mM KCl) were taken with an inverted microscope (Axiovert 200m, Zeiss, Thornwood, NY) operating in phase-contrast mode. An image-processing program (ImageJ, NIH) was used for analysis of the images and for determining the average major and minor axes of the three cell types. The resulting equivalent spherical diameters of D21g, D21f2g, and JM109g were found to be 1.84, 1.77, and 1.46 μm, respectively.

Viability of the cells was determined by use of the BacLight Viability Kit (Molecular Probes, Eugene, OR) under the range of solution conditions tested. This technique allows for direct counting and quantification of the stained live and dead cells with an inverted microscope (Axiovert 200m, Zeiss) operating in fluorescent mode with the appropriate filter set (Chroma Technology Corp, Brattleboro, VT). It was found that, on average,

(26) Coughlin, R. T.; Tonsager, S.; McGroarty, E. J. *Biochemistry* **1983**, *22*, 2002.

(27) Holst, O.; Ulmer, A. J.; Brade, H.; Flad, H. D.; Rietschel, E. T. *FEMS Immunol. Med. Microbiol.* **1996**, *16*, 83.

(28) Kastowsky, M.; Gutberlet, T.; Bradacsek, H. *J. Bacteriol.* **1992**, *174*, 4798.

(29) Burks, G. A.; Velegol, S. B.; Paramonova, E.; Lindenmuth, B. E.; Feick, J. D.; Logan, B. E. *Langmuir* **2003**, *19*, 2366.

(30) Simoni, S. F.; Harms, H.; Bosma, T. N. P.; Zehnder, A. J. B. *Environ. Sci. Technol.* **1998**, *32*, 2100.

(31) Amro, N. A.; Kotra, L. P.; Wadu-Mesthrige, K.; Bulychev, A.; Mobashery, S.; Liu, G. Y. *Langmuir* **2000**, *16*, 2789.

(32) Velegol, S. B.; Logan, B. E. *Langmuir* **2002**, *18*, 5256.

(33) Berlyn, M. B.; Letovsky, S. *Nucleic Acids Res.* **1992**, *20*, 6143.

(34) Boman, H. G.; Monner, D. A. *J. Bacteriol.* **1975**, *121*, 455.

(35) Stuurman, N.; Bras, C. P.; Schlaman, H. R. M.; Wijffes, A. H. M.; Bloemberg, G.; Spaink, H. P. *Mol. Plant–Microbe Interact.* **2000**, *13*, 1163.

(36) Sambrook, J.; Fritsch, E. F.; Maniatis, T. *Molecular Cloning, A Laboratory Manual*; 2nd ed.; Cold Spring Harbor Laboratory Press: Cold Spring Harbor, New York, 1989; Vol. 3.

(37) Ottewill, R. H.; Shaw, J. N. *J. Electroanal. Chem.* **1972**, *37*, 133.

the percent of viable cells was greater than 80% across the various strains and solution ionic strengths examined.

2.3. Collector Quartz Media. Ultrapure quartz collector media were selected for use in experimentation since commonly used collectors—soda lime glass beads or borosilicate microscope coverslips—possess microscopic-scale surface chemical heterogeneities.^{38,39} Such chemical (charge) heterogeneities may have a profound influence on bacterial adhesion behavior.

2.3.1. Granular Porous Medium. Ultrapure quartz sand (Unimin Corp., Spruce Pine, NC) was size-fractionated with nylon sieves (U.S. standard mesh sizes of 60 and 100, which correspond to 250- and 150- μm openings, respectively) for use as a packing material for column experiments. Prior to use, the sand was cleaned thoroughly to remove metal and organic impurities by soaking the sand in 12 N HCl (Fisher) for at least 24 h, washing in deionized water (Barnstead), and baking at 800 °C for 8 h minimum.⁴⁰ Before being packed in the column, the cleaned sand was rehydrated by boiling in deionized water for 1 h. Sieve analysis resulted in an average grain diameter (d_{50}) of 205 μm . For column experiments under nonrepulsive electrostatic conditions (so-called “favorable” deposition), the surface charge of the quartz sand was modified via reaction with aminosilane molecules. Silanization involved suspension of the quartz grains in a 1% (v/v) solution of (3-aminopropyl)triethoxysilane (Sigma) for 5 min, followed by thorough rinsing in deionized water and curing at 80 °C for 24 h.

2.3.2. Quartz Coverslip. Round quartz coverslips of 25 mm diameter and 0.1 mm thickness (Electron Microscopy Sciences, Ft. Washington, PA) were used in the radial stagnation point flow (RSPF) deposition experiments. Prior to use, the coverslips were cleaned by soaking in a 2% Extran MA02 solution (EM Science, Gibbstown, NJ), followed by a thorough rinsing with ethanol (Pharmco Products, Inc. Brookfield, CT) and deionized water. Next, the quartz slips were sonicated (10–15 min) while submerged in a 2% RBS 35 detergent solution (Pierce, Rockford, IL), followed by a second rinsing with ethanol and DI water. The coverslips were soaked overnight in Nochromix solution (Godax Laboratories, Inc., Tacoma Park, MD) and then rinsed thoroughly with deionized water. For favorable deposition experiments (i.e., in the absence of repulsive electrostatic interactions), the slides were chemically modified with aminosilane. In this surface modification procedure, one side of the quartz coverslip was exposed to a 0.2% (v/v) mixture of (aminoethylaminomethyl)-phenethyltrimethoxysilane (Gelest, Inc., Tullytown, PA) in ethanol for 3–5 min at room temperature and then cured for 90 min at 130 °C.

2.3.3. Electrokinetic Characterization of Quartz Grains and Coverslips. The electrokinetic properties of the collector surfaces were determined by a streaming potential analyzer (EKA, Brookhaven Instruments Corp.). A cylindrical cell, packed to a bed depth of 3 cm, was used for the quartz sand,³⁸ while an asymmetric clamping cell was used to measure the streaming potential of the quartz coverslip.⁴¹ Measurements were conducted over a range of ionic strengths, from 10⁻³ to 10⁻¹ M KCl, at an unadjusted pH (about 5.7) and room temperature (22 °C). In both measuring cells, the instrument was first rinsed extensively with deionized water (1 L), followed by the electrolyte solution used in measurement (0.5 L), and finally the sample was equilibrated with fresh electrolyte solution (0.5 L) for 10 min. The ζ potential was calculated from the measured streaming potentials as described elsewhere.^{38,41}

2.4. Packed-Bed Column Experiments. Bacterial transport experiments were conducted in glass chromatography columns packed with clean quartz grains. Adjustable bed height columns (Omnifit USA, Toms River, NJ) with a 1 cm inner diameter were used. Columns were wet-packed by allowing the quartz grains to settle in deionized water while the column was agitated. Porosity of the packed columns was determined gravimetrically

to be 0.43. Prior to each experiment, the packed column was equilibrated by sequentially pumping (Model 200 syringe pump, KD Scientific Inc., New Hope, PA) 10 pore volumes of deionized water followed by 10 pore volumes of the background electrolyte solution. The ionic strength of the pore fluid, adjusted by addition of KCl, ranged from 10⁻³ to 10^{-0.5} M. A typical experiment involved pumping bacterial cells suspended in an electrolyte solution (10⁷–10⁸ cells/mL) through the column for 15 min (approximately 4 pore volumes) followed by a bacteria-free solution of the same electrolyte composition for at least 45 min (approximately 12 pore volumes). The approach (superficial) velocity during the column experiments was fixed at 0.021 cm/s.

Selected experiments designed to investigate the release of previously deposited bacteria involved the injection of an additional pulse of a bacteria-free low ionic strength solution (10⁻⁴ MKCl). In these experiments, the fraction of eluted bacteria is defined as the ratio of the amount of eluted cells to the amount of deposited cells. The amount of deposited cells was determined by taking the difference between the total amount injected into the column and the numerically integrated amount eluted over all pore volumes up to the injection of the low ionic strength solution. The amount of bacteria released from the column was determined by numerically integrating over all pore volumes from the time of the elution solution injection until the cell concentration had decayed to background levels.

The bacterial cell concentration in the column effluent was monitored at 2-s intervals by measuring the absorbance at 280 nm with a UV/vis spectrophotometer (Hewlett-Packard model 8453) and a 1-cm flow-through cell. After each experiment (ca. 1–1.5 h), the bacterial cell solution was connected directly to the flow-through cell for determination of the influent concentration. All solutions had an unadjusted pH between 5.6 and 5.8 at room temperature (22 °C). The length of the packed beds for the column experiments was adjusted between 7 and 20 cm to obtain absorbance readings that were within the detection range of the spectrophotometer.

2.5. Radial Stagnation Point Flow Experiments. To better understand bacterial adhesion mechanisms under flow conditions, deposition experiments were conducted in a well-controlled radial stagnation point flow (RSPF) system. This system is composed of a specially blown glass flow chamber installed on the stage of an inverted fluorescent microscope (Axiovert 200m, Zeiss). The bacterial suspension entered the radially symmetric flow cell through a capillary tube oriented in a downward direction (2 mm inner diameter). Flow impinged upon a microscope cover glass 2 mm below the capillary opening and traveled radially along the cover slide, exiting the RSPF chamber through a separate capillary tube. An LD Achromplan 40 \times objective (1.8 mm working distance) located beneath the flow cell was focused on the inner surface of the quartz coverslip. The fluorescent cells were imaged by use of a fluorescent filter set with an excitation wavelength of 480 nm and emission wavelength of 510 nm (Chroma Technology Corp). Deposition of bacterial cells was recorded with a digital camera (AxioCam MR monochrome, Zeiss), acquiring images every 20 s over the course of a 20 min injection, and analyzed with the supplied software (AxioVision 3.1, Zeiss). The number of deposited bacterial cells was determined for each image by comparing the changes between successive images.

Bacterial cell deposition experiments in the RSPF system were conducted over a range of ionic strength (KCl) conditions with a cell concentration of 10⁷–10⁸ cells/mL. For each deposition run, the influent cell concentration was determined directly by visualizing cells in a counting chamber (Buerker-Tuerk chamber, Marienfeld Laboratory Glassware, Lauda-Königshofen, Germany). A flow rate of 5 mL/min was used, resulting in particle Peclet numbers⁴² comparable to those in the packed column.

3. Results and Discussion

3.1. Bacterial Cell Selection. The presence and structure of lipopolysaccharides (LPS) on the outer membrane of *E. coli* K12 have been studied exten-

(38) Elimelech, M.; Nagai, M.; Ko, C. H.; Ryan, J. N. *Environ. Sci. Technol.* **2000**, *34*, 2143.

(39) Dong, H. L.; Onstott, T. C.; Deflaun, M. F.; Fuller, M. E.; Scheibe, T. D.; Streger, S. H.; Rothmel, R. K.; Mailloux, B. J. *Environ. Sci. Technol.* **2002**, *36*, 891.

(40) Litton, G. M.; Olson, T. M. *Environ. Sci. Technol.* **1993**, *27*, 185.

(41) Walker, S. L.; Bhattacharjee, S.; Hoek, E. M. V.; Elimelech, M. *Langmuir* **2002**, *18*, 2193.

(42) Elimelech, M.; Gregory, J.; Jia, X.; Williams, R. A. *Particle Deposition and Aggregation: Measurement, Modeling and Simulation*; Butterworth-Heinemann: Woburn, MA, 1995.

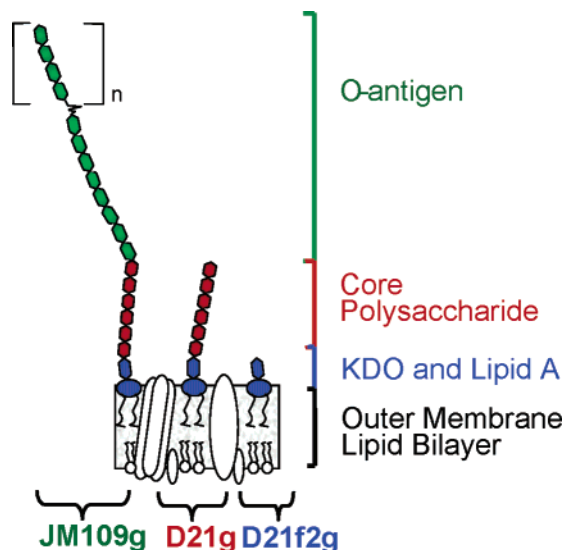


Figure 1. Schematic diagram of the structure of the lipopolysaccharide (LPS) molecule on each of the three *E. coli* strains used in this investigation.

sively.^{28,31,34} In this particular study, mutants of the *E. coli* K12 have been selected to systematically study the role of LPS in cell adhesion and transport. Specifically, three strains were selected—D21g, D21f2g, and JM109g—on the basis of the specific structure and length of the LPS molecule on each strain (Figure 1). The three mutants are particularly suitable for our study due to their lack of flagella or natural motility.⁴³ The mutants were transformed to express an enhanced green fluorescent protein (EGFP), as indicated by the letter g at the end of the strain name.

The D21f2g strain has the most truncated form of the LPS molecule, consisting of the outer lipid of the membrane and an exposed hydrophilic KDO molecule attached to the outer lipid of the membrane. The D21g strain has an intermediate-length LPS molecule, comprising the lipid and KDO molecules as well as the core polysaccharide region. Finally, the JM109g strain contains the full LPS molecule, which includes the lipid, KDO, core polysaccharide, and an extended polysaccharide chain, referred to as the O-antigen. It has been reported that the core polysaccharide consists of six- and seven-carbon sugar group chains, totaling 2–3 nm in length.²⁸ The O-antigen is composed of primarily six-carbon sugars connected in repeating branched or straight sequences up to approximately 40 nm in length.²⁵ Sensitivity to growth conditions and solution chemistry controls the conformation of the LPS, leaving the exact length that the LPS molecule extends into the aqueous solution undefined.

3.2. Electrokinetic Properties of Bacterial Cells and Collector Surfaces. The outer membranes of Gram-negative bacteria contain membrane-bound proteins and LPS that can ionize and give rise to a pH-dependent net surface charge.¹⁵ It is well documented that the net charge of bacterial cells in natural aquatic systems is negative.^{44–46} As illustrated in Figure 2a, the three strains used in this study are negatively charged at the examined pH (5.6–5.8). For all strains, the absolute magnitude of the cell ζ

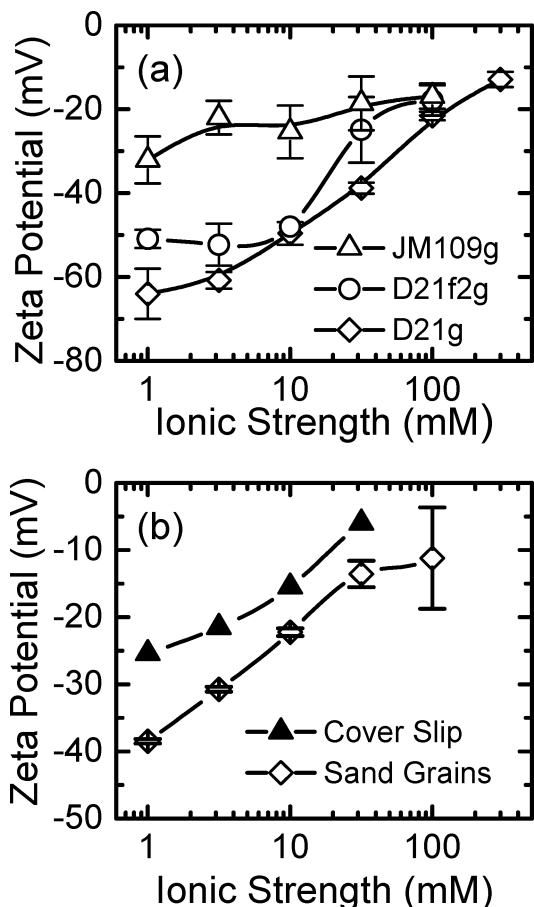


Figure 2. Zeta (ζ) potential as a function of ionic strength for (a) the three *E. coli* strains and (b) the quartz grains and coverslips. Measurements were carried out at an unadjusted pH of 5.6–5.8. Error bars indicate one standard deviation.

potential decreased with an increase in salt (KCl) concentration as expected from electrostatic double-layer compression with a 1:1 electrolyte. The cell type with the least negative ζ potential was JM109g, while the most negative potential was found for D21g. Although slightly less negative, the ζ potential of D21f2g was closer to that of D21g.

The LPS of D21g has a greater number of negatively charged functional groups than D21f2g due to the presence of three additional phosphate groups in the core region.^{26,47} These functional groups can ionize and contribute to the net negative charge on the membrane surface under the solution chemistry conditions tested. It has been reported that the charged phosphate residues originate from substitution of heptose and KDO in the core polysaccharide region.²⁴ Despite the differences in magnitude, the similar shape of the ζ potential profiles of D21g and D21f2g may be related to their being mutants of the same parent cell.³⁴ JM109g, on the other hand, has a notably less negative ζ potential and is derived from a separate *E. coli* K12 mutant strain. This lower negative ζ potential of JM109g is most likely attributed to the relatively long uncharged O-antigen, shielding charge and shifting the electrokinetic plane of shear. The different ancestry of JM109g may also result in variations in the membrane-bound proteins and core polysaccharide structure compared to the isogenic mutants D21g and D21f2g.

The ζ potential of the quartz surfaces is presented in Figure 2b. Both the quartz grains and the quartz

(43) Jones, J. F.; Feick, J. D.; Imoudu, D.; Chukwumah, N.; Vigeant, M.; Velegol, D. *Appl. Environ. Microbiol.* **2003**, *69*, 6515.

(44) Rijnaarts, H. H. M.; Norde, W.; Lyklema, J.; Zehnder, A. J. B. *Colloid Surf. B—Biointerfaces* **1995**, *4*, 191.

(45) van der Wal, A.; Minor, M.; Norde, W.; Zehnder, A. J. B.; Lyklema, J. *Langmuir* **1997**, *13*, 165.

(46) Sokolov, I.; Smith, D. S.; Henderson, G. S.; Gorby, Y. A.; Ferris, F. G. *Environ. Sci. Technol.* **2001**, *35*, 341.

(47) Gmeiner, J.; Schlecht, S. *Arch. Microbiol.* **1980**, *127*, 81.

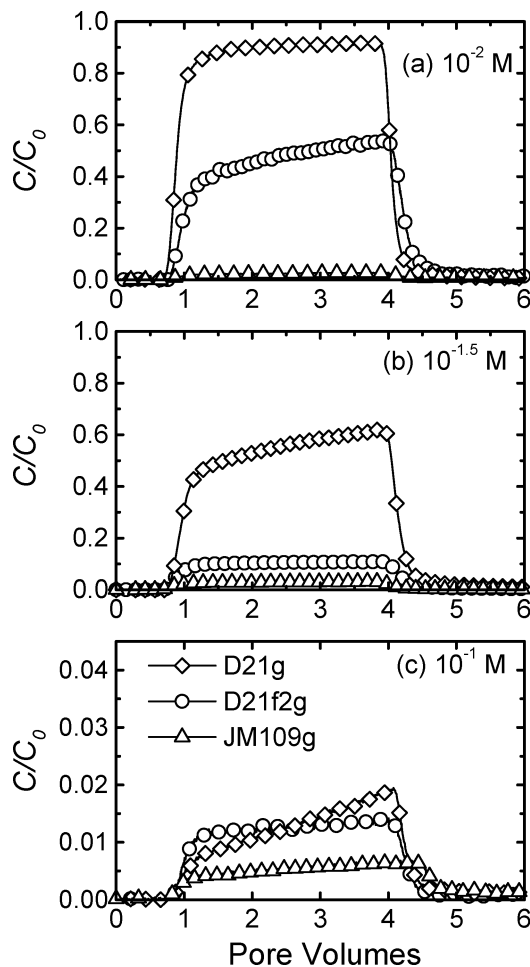


Figure 3. Normalized effluent concentration (C/C_0) of the three bacterial strains as a function of pore volume for three representative solution ionic strengths: (a) 10^{-2} M KCl, (b) $10^{-1.5}$ M KCl, and (c) 10^{-1} M KCl. For clarity, every 20th data point is plotted. Note the scale for C/C_0 at 10^{-1} M KCl is different than the other ionic strengths because of extensive bacterial retention in the column. Experimental conditions are as follows: approach velocity = 0.021 cm/s, porosity = 0.43, mean grain diameter = 205 μm , and pH = 5.6–5.8.

microscope coverslip are negatively charged at the examined pH (5.6–5.8). Hence, electrostatic double-layer repulsion prevails in the bacterial adhesion experiments. The ζ potentials presented in Figure 2 are used later in this paper for DLVO interaction energy calculations to delineate the mechanisms involved in cell adhesion to the quartz surfaces.

3.3. Bacterial Transport and Deposition. The packed-bed column system is commonly used to study bacterial adhesion, as it captures the macroscopic behavior of bacterial transport and adhesion relevant to many engineered and natural processes (e.g., packed-bed filters and subsurface porous media). To examine the kinetics of bacterial deposition (adhesion) at the microscopic level, a radial stagnation point flow (RSPF) system was used.

3.3.1. Packed-Bed Column Experiments. The adhesion and transport of the three *E. coli* strains were systematically examined over a wide range of solution ionic strengths. Sample breakthrough curves illustrating the influence of ionic strength on cell transport are shown in Figure 3. The normalized effluent concentration of each cell type is plotted against the number of pore volumes passed through the column at three representative solution ionic strengths. After approximately 1–2 pore volumes, the injected bacteria break through the packed

bed and are detected in the effluent. After 4 pore volumes, the influent is switched to a bacteria-free solution of identical ionic strength and the concentration of bacteria in the effluent decreases continuously until it eventually approaches zero. Most transport experiments were replicated between four and six times for each cell type and ionic strength. The calculated deposition rate coefficients (to be discussed below) from these experiments are presented in Table 1 for the range of ionic strength conditions investigated.

As seen in Figure 3a,b, an increase in the pore fluid ionic strength from 10^{-2} to $10^{-1.5}$ M KCl results in increased retention of all three *E. coli* strains, although at these intermediate ionic strengths the retention behavior for each strain is distinct. The differences in bacterial retention become less pronounced at the higher ionic strength, as seen in Figure 3c. Once the pore fluid ionic strength reaches a sufficiently high level, such as 10^{-1} M KCl, the normalized breakthrough concentrations appear to converge to a very low value. The observed behavior of increased bacterial removal (i.e., lower C/C_0) with increasing ionic strength is in qualitative agreement with expectations based on reduction of electrostatic double-layer repulsion with ionic strength.

To quantitatively compare the deposition (adhesion) kinetics of the three *E. coli* strains at different solution ionic strengths, the deposition rate coefficient k_d was determined:⁴⁸

$$k_d = -\frac{U}{fL} \ln\left(\frac{C}{C_0}\right) \quad (1)$$

Here, C/C_0 is the normalized breakthrough concentration relevant to “clean bed” conditions, U is the approach (superficial) fluid velocity, f is the packed-bed porosity, and L is the length of the packed bed. In a few experiments (e.g., D21g at $10^{-1.5}$ M), the normalized cell concentration did not attain a steady-state value following the initial dispersive region of breakthrough. The slow increase of concentration with time indicates either “blocking” by previously deposited bacterial cells⁴⁹ or simultaneous bacterial deposition and release.⁵⁰ Hence, the “clean bed” C/C_0 was determined for each experiment by averaging the normalized breakthrough concentrations measured between 1.8 and 2 pore volumes.

In general, an increase in ionic strength of the pore fluid results in a higher deposition rate coefficient, k_d . As can be seen in Figure 4, there is approximately a 2 orders of magnitude increase in deposition rate over the range of examined salt concentrations for D21g and D21f2g. On the other hand, the deposition rate of JM109g exhibits a distinct trend, where k_d is relatively unchanged above $10^{-2.5}$ M but decreases by an order of magnitude when the ionic strength is lowered from $10^{-2.5}$ to 10^{-3} M. The trends in the deposition rates of the three strains are consistent with their ζ potential behavior (Figure 2), reflecting the paramount role of electrostatic double-layer repulsion. The most negatively charged bacterial strain (D21g) exhibited the lowest deposition rate, whereas the least negatively charged strain (JM109g) displayed the highest deposition rate. There appears to be no relation between LPS length and deposition rate, although it is noted that the strain

(48) Kretzschmar, R.; Borkovec, M.; Grolimund, D.; Elimelech, M. *Adv. Agron.* **1999**, *66*, 121.

(49) Camesano, T. A.; Unice, K. M.; Logan, B. E. *Colloid Surf. A* **1999**, *160*, 291.

(50) Meinders, J. M.; van der Mei, H. C.; Busscher, H. J. *J. Colloid Interface Sci.* **1995**, *176*, 329.

Table 1. Comparison of Deposition Rates and Attachment Efficiencies Calculated from Packed-Bed and Radial Stagnation Point Flow Experiments

strain	ionic strength (M)	packed bed		RSPF	
		k_d (s ⁻¹)	α_{col}	k_{RSPF} (m/s)	α_{RSPF}
D21f2g	10 ^{-3.0}	$(1.3 \pm 0.4) \times 10^{-4}$ ($n = 3$)	$(3.6 \pm 1.1) \times 10^{-3}$	NM ^a	NM
D21f2g	10 ^{-2.5}	$(6.1 \pm 7) \times 10^{-4}$ ($n = 2$)	$(1.8 \pm 2.0) \times 10^{-2}$	NM	NM
D21f2g	10 ^{-2.0}	$(2.1 \pm 0.5) \times 10^{-3}$ ($n = 3$)	$(6.2 \pm 1.4) \times 10^{-2}$	NM	NM
D21f2g	10 ^{-1.5}	$(1.2 \pm 0.3) \times 10^{-2}$ ($n = 5$)	$(3.5 \pm 0.9) \times 10^{-1}$	$(5.7 \pm 3.6) \times 10^{-9}$ ($n = 4$)	$(5.48 \pm 3.5) \times 10^{-2}$
D21f2g	10 ^{-1.0}	$(1.7 \pm 0.1) \times 10^{-2}$ ($n = 4$)	$(4.8 \pm 0.4) \times 10^{-1}$	$(3.3 \pm 0.5) \times 10^{-8}$ ($n = 2$)	$(3.16 \pm 0.5) \times 10^{-1}$
D21f2g	10 ^{-0.5}	$(3.7 \pm 0.2) \times 10^{-2}$ ($n = 2$)	1.1 ± 0.04	ND ^b	ND
D21g	10 ^{-3.0}	$(9.6 \pm 5.7) \times 10^{-5}$ ($n = 4$)	$(2.7 \pm 1.6) \times 10^{-3}$	NM	NM
D21g	10 ^{-2.5}	$(1.8 \pm 0.4) \times 10^{-4}$ ($n = 4$)	$(5.1 \pm 1.3) \times 10^{-3}$	NM	NM
D21g	10 ^{-2.0}	$(5.2 \pm 1.3) \times 10^{-4}$ ($n = 5$)	$(1.5 \pm 0.4) \times 10^{-2}$	NM	NM
D21g	10 ^{-1.5}	$(2.3 \pm 0.6) \times 10^{-3}$ ($n = 7$)	$(6.6 \pm 1.6) \times 10^{-2}$	$(7.7 \pm 3.2) \times 10^{-10}$ ($n = 3$)	$(3.13 \pm 1.3) \times 10^{-3}$
D21g	10 ^{-1.0}	$(1.8 \pm 0.2) \times 10^{-2}$ ($n = 5$)	$(5.1 \pm 0.7) \times 10^{-1}$	$(5.6 \pm 1.4) \times 10^{-9}$ ($n = 6$)	$(2.27 \pm 0.6) \times 10^{-2}$
D21g	10 ^{-0.5}	3.1×10^{-2} ($n = 1$)	8.9×10^{-1}	$(4.7 \pm 2.5) \times 10^{-8}$ ($n = 3$)	$(1.91 \pm 1.0) \times 10^{-1}$
JM109g	10 ^{-3.0}	$(5.6 \pm 2.6) \times 10^{-4}$ ($n = 2$)	$(8.9 \pm 3.6) \times 10^{-3}$	NM	NM
JM109g	10 ^{-2.5}	$(6.5 \pm 2.5) \times 10^{-3}$ ($n = 4$)	$(1.0 \pm 0.4) \times 10^{-1}$	NM	NM
JM109g	10 ^{-2.0}	$(1.2 \pm 0.5) \times 10^{-2}$ ($n = 6$)	$(1.9 \pm 0.8) \times 10^{-1}$	NM	NM
JM109g	10 ^{-1.5}	$(1.4 \pm 0.3) \times 10^{-2}$ ($n = 4$)	$(2.3 \pm 0.4) \times 10^{-1}$	$(6.8 \pm 3.5) \times 10^{-8}$ ($n = 3$)	$(2.54 \pm 1.0) \times 10^{-1}$
JM109g	10 ^{-1.0}	1.8×10^{-2} ($n = 1$)	2.9×10^{-1}	$(1.6 \pm 0.7) \times 10^{-7}$ ($n = 2$)	$(6.01 \pm 2.1) \times 10^{-1}$
JM109g	10 ^{-0.5}	3.1×10^{-2} ($n = 1$)	4.9×10^{-1}	ND	ND

^a No measurable bacterial deposition. ^b Not determined.

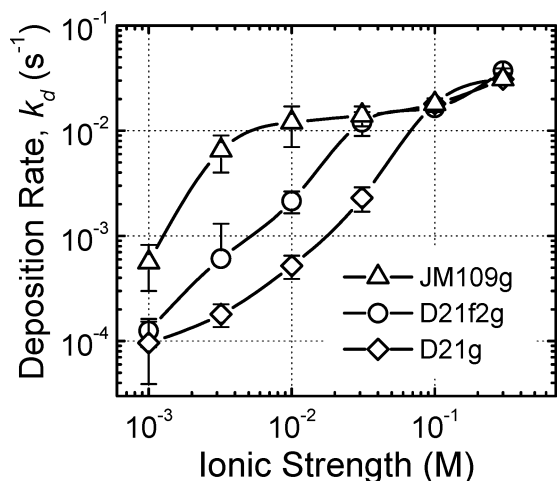


Figure 4. Variation of bacterial deposition rate coefficient with ionic strength for the three *E. coli* strains. The deposition rate coefficients were calculated from replicate breakthrough curves (summarized in Table 1) under experimental conditions similar to those outlined in Figure 3. Error bars indicate one standard deviation.

with the longest LPS, JM109g, appears to be the most adhesive. This observation will be discussed later in the paper.

3.3.2. Radial Stagnation Point Flow Experiments.

The packed column system is an *indirect* technique to study bacterial adhesion and, thus, does not allow the investigation of microscopic bacterial adhesion and transport mechanisms. To overcome this difficulty, a radial stagnation point flow (RSPF) system was utilized for *direct* microscopic observation of bacterial deposition kinetics. The RSPF system eliminates the effect of quartz grain geometry (irregular shape and roughness) and allows for the visualization of bacterial cell adhesion onto a single, well-defined collector rather than through an assemblage of packed collectors with a complex flow behavior.

The RSPF system was designed to complement the packed-bed column experiments. Specifically, a highly cleaned quartz coverslip was used as the collector surface to closely mimic the DLVO interactions within the packed-bed column. In addition, the hydrodynamic conditions in the RSPF and packed-bed column were adjusted such that the particle Peclet numbers were comparable. The cor-

responding particle Peclet numbers for the packed bed, Pe_{PB} , and the RSPF system, Pe_{RSPF} , were calculated from⁴²

$$Pe_{PB} = \frac{3A_s U a_p^3}{D_\infty a_c^2} \quad (2)$$

$$Pe_{RSPF} = \frac{\hat{\alpha}_{RSPF} V_0 a_p^3}{D_\infty R^2} \quad (3)$$

Here, A_s is a porosity-dependent parameter for the Happel model ($A_s = 31.71$ for a porosity of 0.43), U is the superficial (approach) fluid velocity in the packed column, a_p is the average bacterial radius, D_∞ is the cell bulk diffusion coefficient, a_c is the average radius of the quartz collector, $\hat{\alpha}_{RSPF}$ is a numerical function accounting for the hydrodynamics and geometry of the RSPF system, V_0 is the average velocity in the capillary (flow rate divided by capillary cross-sectional area), and R is the radius of the capillary.

The bacterial deposition kinetics in the RSPF system are quantified by calculating a bacterial transfer rate coefficient, k_{RSPF} :

$$k_{RSPF} = \frac{J}{C_0} \quad (4)$$

where C_0 is the bacterial bulk concentration and J is the deposition flux of bacteria to the coverslip. To determine the deposition flux, J , the observed deposition rate of bacteria on the coverslip (i.e., the initial slope of the number of deposited bacteria versus time) was normalized by the microscope viewing area ($210 \times 165 \mu\text{m}$).

The influence of ionic strength on k_{RSPF} is shown in Figure 5. The bacterial transfer rate to the collector surface increased with increasing ionic strength for D21g, D21f2g, and JM109g between $10^{-1.5}$ and 10^{-1} M. Below $10^{-1.5}$ M the deposition rate of the three strains could not be measured, as there was negligible deposition over the course of the experiment. Replicate experiments below $10^{-1.5}$ M resulted in an average of less than one cell depositing over the 20 min of imaging, even with bulk cell concentrations up to 10^8 cells/mL. As with the packed-bed results, the deposition behavior of the *E. coli* strains is consistent with the observed trends in ζ potential. This

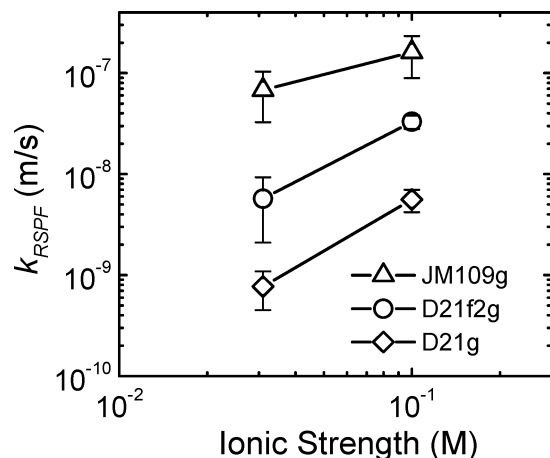


Figure 5. Bacterial deposition kinetics in the radial stagnation point flow system, presented as the cell transfer rate coefficient, k_{RSPF} , as a function of ionic strength for each of the three *E. coli* strains. Experimental conditions are as follows: RSPF capillary flow velocity = 0.0265 m/s and pH = 5.6–5.8. Error bars indicate one standard deviation.

suggests that the decrease in electrostatic repulsion between the bacteria and quartz surface results in greater adhesion.

Additional interpretation of the bacterial deposition kinetics data shown in Figures 4 and 5 is given in the following sections. More specifically, we will use classic DLVO theory to analyze the dependence of bacterial deposition rate on ionic strength. Furthermore, the different hydrodynamics in the packed-bed column and RSPF system will be exploited to identify the mechanisms dominating bacterial deposition under dynamic flow conditions.

3.4. Bacterial Adhesion Dependence on Electrostatic Interactions. As shown earlier in Figure 2, both the quartz collector surfaces and the bacterial cells are negatively charged at the conditions of our study. Thus, it is expected that electrostatic repulsion would inhibit adhesion, at least at the moderate and low ionic strength conditions. Experiments, however, indicate that significant bacterial adhesion in the packed beds is not only occurring but increasing with ionic strength. Therefore, we apply classical DLVO theory to explain the deposition behavior and elucidate the mechanisms controlling bacterial cell adhesion to quartz surfaces in our experimental systems.

3.4.1. DLVO Interaction Profiles. A sample plot of interaction energy versus separation distance for the *E. coli* D21f2g strain at various ionic strengths is shown in Figure 6. Calculated interaction profiles are based on the ζ potentials in Figure 2, a value of the Hamaker constant of 6.5×10^{-21} J,^{51,52} and an equivalent bacterial cell radius of 0.885 μm . Repulsive electrostatic interaction energy was determined from the constant surface potential equation of Hogg et al.,⁵³ while the retarded van der Waals expression of Gregory⁵⁴ was used to determine the attractive interaction contribution. A sphere-plate geometry was assumed when the interaction energies are calculated.

The DLVO profiles reveal the existence of a significant energy barrier at ionic strengths between 10^{-3} and $10^{-1.5}$

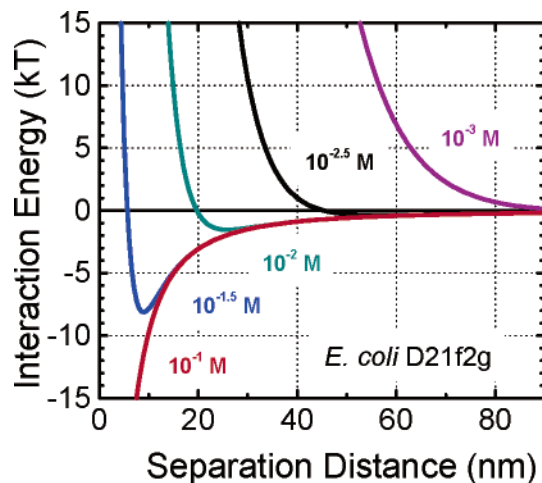


Figure 6. Calculated DLVO interaction energies as a function of separation distance and molar ionic strength (indicated next to each curve) for *E. coli* D21f2g. Interaction energies were calculated by use of the ζ potentials (Figure 2) as surface potentials. The Hamaker constant for the bacteria–water–quartz interacting media was assumed to be 6.5×10^{-21} J (see discussion in text). An equivalent bacterial cell radius of 0.885 μm was used in the calculations.

M. Specifically, the energy barrier varied from approximately 2000 kT at 10^{-3} M to 81 kT at $10^{-1.5}$ M. These insurmountable energy barriers suggest that bacterial deposition in primary minima is unlikely. However, a close inspection of the DLVO profiles in Figure 6 reveals the existence of a secondary energy minimum. As the ionic strength increases, the secondary energy well gets deeper and closer to the surface. Such interaction energy profiles suggest that bacterial cells can be captured in secondary energy minima.^{55–57} A bacterial cell will remain associated with the collector surface in this energy minimum unless it has sufficient energy to allow the cell to escape.⁵⁷ As demonstrated in our column experiments, the deposition behavior qualitatively agrees with the observed trends of increasing depth of the secondary minimum with ionic strength.

Table 2 summarizes the key DLVO calculations for the three *E. coli* strains. Results reveal similar trends in secondary minima depth and separation distances for all three strains. This lack of distinction is because the small differences in cell size and ζ potential have a minimal effect on the calculated location and depth of the secondary energy minima. Although DLVO calculations do not capture the subtleties between strains, the deposition rates (both k_d and k_{RSPF}) do show substantial differences. This indicates that interaction energy profiles alone are insufficient to quantitatively explain the differences in deposition trends between the three *E. coli* strains.

3.4.2. Correlation of Adhesion with DLVO Interactions. To further characterize the mechanisms governing bacterial adhesion, a dimensionless parameter, N_{DLVO} , was calculated.⁵⁸ This parameter incorporates the factors controlling the height of the DLVO energy barrier as well as the depth of the secondary energy minimum:

(51) Simoni, S. F.; Bosma, T. N. P.; Harms, H.; Zehnder, A. J. B. *Environ. Sci. Technol.* **2000**, *34*, 1011.

(52) Truesdail, S. E.; Lukasik, J.; Farrah, S. R.; Shah, D. O.; Dickinson, R. B. *J. Colloid Interface Sci.* **1998**, *203*, 369.

(53) Hogg, R.; Healy, T. W.; Fuersten, D. W. *Trans. Faraday Soc.* **1966**, *62*, 1638.

(54) Gregory, J. *J. Colloid Interface Sci.* **1981**, *83*, 138.

(55) Redman, J. A.; Walker, S. L.; Elimelech, M. *Environ. Sci. Technol.* **2004**, *38*, 1777–1785.

(56) Jucker, B. A.; Harms, H.; Zehnder, A. J. B. *Colloid Surf. B–Biointerfaces* **1998**, *11*, 33.

(57) Hahn, M. W.; O'Melia, C. R. *Environ. Sci. Technol.* **2004**, *38*, 210.

(58) Elimelech, M. *Water Res.* **1992**, *26*, 1.

Table 2. Calculated Secondary Minimum Depth and Separation Distance between the Collector Surface and the Three Bacterial Strains as a Function of Solution Ionic Strength^a

ionic strength (M)	D21g		D21f2g		JM109g	
	depth (kT)	distance (nm)	depth (kT)	distance (nm)	depth (kT)	distance (nm)
10 ^{-3.0}	0.1	120	0.1	118	0.1	112
10 ^{-2.5}	0.4	58	0.4	57	0.4	51
10 ^{-2.0}	1.6	26	1.5	26	1.5	23
10 ^{-1.5}	7.1	10	8.1	9	7.7	8
10 ^{-1.0}	NS ^b	NS	NS	NS	NS	NS

^a A Hamaker constant of 6.5×10^{-21} J and cell diameters of 1.84, 1.77, and 1.46 μm for D21g, D21f2g, and JM109g, respectively, were assumed. ^b No secondary energy minimum existed for the three bacterial strains at 10^{-1} M.

$$N_{\text{DLVO}} = \frac{\kappa A}{\epsilon_0 \epsilon_r \psi_p \psi_c} \quad (5)$$

Here, ψ_p and ψ_c are the surface potentials of the bacterial cells and quartz collectors, respectively, κ is the inverse Debye length characterizing the range of electrostatic double-layer interactions, A is the Hamaker constant of the interacting media, ϵ_0 is the dielectric permittivity of a vacuum, and ϵ_r is the relative dielectric permittivity of water. N_{DLVO} was determined for each of the ionic strength conditions and cell types used in the packed column experiments, with ζ potentials for both the cells and quartz grains used in place of surface potentials.

Figure 7 presents the resulting relationship between N_{DLVO} and the bacterial deposition rate coefficients (k_d) determined for the column experiments, revealing distinct trends for the three bacterial strains. For all strains, an increase in N_{DLVO} —reflecting a decrease in electrostatic repulsive forces and a concomitant increase in the depth of the secondary minimum—results in a corresponding increase in the deposition rate. Over the range of ionic strengths considered, D21g shows linear dependence (on a log–log plot) of the bacterial deposition rate coefficients on the dimensionless N_{DLVO} parameter, strongly suggesting that DLVO forces dominate the D21g–quartz grain interaction. Although less linear, the deposition rate coefficient of D21f2g also exhibits clear dependence on the N_{DLVO} parameter. This is indicated by the deposition rate increasing 2 orders of magnitude with increasing N_{DLVO} , at virtually the same rate as D21g. The only notable difference between these two strains occurs at the highest ranges of N_{DLVO} , where the deposition rate of D21f2g becomes insensitive to ionic strength as shown earlier in Figure 4. This may be attributed to the nonuniform distribution of charged functional groups exposed on the outer cell membrane of D21f2g (discussed later in the paper), becoming masked at the higher range of ionic strength conditions. D21g, on the other hand, is more sensitive to the subtle changes in solution ionic strength and resulting influence on N_{DLVO} , due to the greater number of negatively charged functional groups on the LPS as indicated by the ζ potentials shown in Figure 2.

The k_d versus N_{DLVO} trend for JM109g was markedly different from the other two strains. Whereas the value of k_d increases in magnitude across the range of N_{DLVO} values for D21g and D21f2g, the increase for JM109g is considerably less. In fact, the deposition rate of this strain appears to be insensitive to N_{DLVO} at ionic strengths greater than $10^{-2.5}$ M. This behavior is in accord with the dependence of k_d on ionic strength (Figure 4) and is likely ascribed to the presence of the O-antigen. Further discussion on the role of the O-antigen in bacterial adhesion is given later in this paper.

3.5. Evidence for Bacterial Deposition in Secondary Minima. Our analysis discussed above illustrates that the bacterial deposition rate on quartz grains

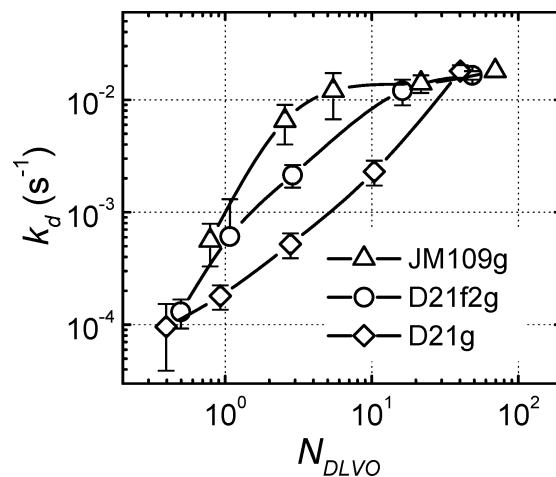


Figure 7. Dependence of the bacterial deposition rate coefficients, k_d , on the dimensionless DLVO parameter, N_{DLVO} , calculated for each ionic strength used in the column experiments. N_{DLVO} was calculated by use of the relevant ζ potentials (in place of surface potentials) and assuming a value of the Hamaker constant of 6.5×10^{-21} J. Error bars indicate one standard deviation.

increases with ionic strength, paralleling the increase in calculated secondary energy minimum depth (Table 2). It was suggested that in the presence of a sizable electrostatic energy barrier, deposition is not occurring in the primary energy minimum at the quartz grain surface but rather predominantly in the secondary energy minimum. To verify the role of the secondary energy minimum in bacterial adhesion, supporting experimentation was conducted in both the packed-bed column and the radial stagnation point flow systems as described below.

3.5.1. Reversibility of Bacterial Adhesion in Packed Beds. To investigate whether the bacterial cells retained in the packed-bed column were indeed deposited in secondary energy minima, release (mobilization) experiments were conducted. Packed-bed column experiments were performed as before, in which cells were deposited at moderate to high ionic strengths (10^{-2} – $10^{-0.5}$ M KCl). After the deposition experiment, a solution of 10^{-4} M KCl was applied to induce release of previously deposited cells. DLVO calculations indicate that this low ionic strength is sufficient to eliminate the secondary energy minimum, thus releasing deposited bacteria captured in this energy well.

A representative breakthrough curve illustrating bacterial elution is presented in Figure 8. Shown are the breakthrough curve and the pulse of released D21f2g cells during an elution experiment. As can be seen, a pulse of released bacteria is eluted from the column beginning about 1 pore volume after the 10^{-4} M KCl solution was applied. The amount of bacterial cells deposited on the quartz grains prior to the injection of the 10^{-4} M KCl

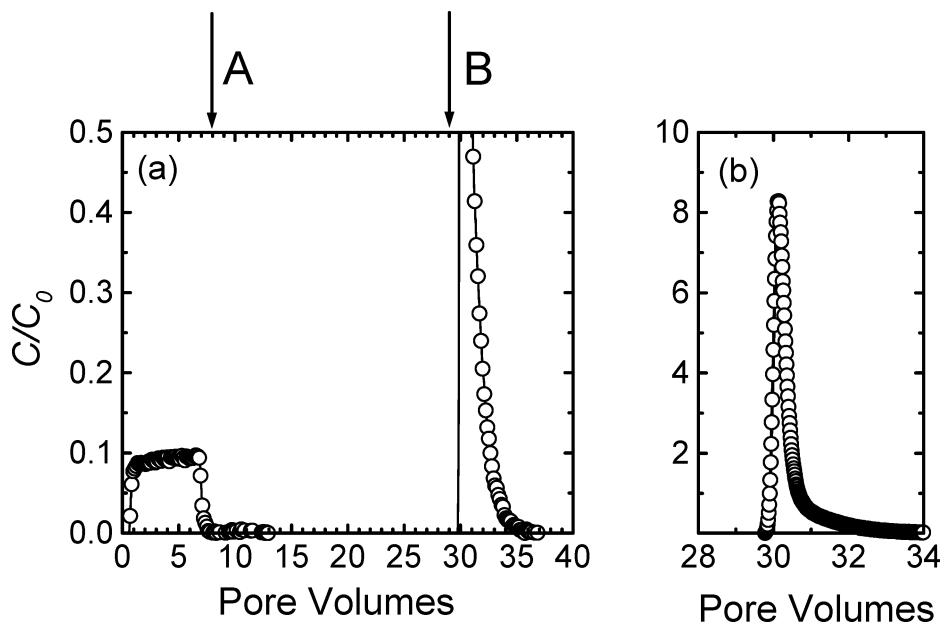


Figure 8. Release of previously deposited D21f2g bacteria induced by pore-fluid ionic strength reduction. Bacteria are initially applied to the column in a $10^{-1.5}$ M KCl solution. Arrows indicate (A) application of $10^{-1.5}$ M bacteria-free solution and (B) application of low ionic strength (10^{-4} M KCl) bacteria-free solution. Note the scale for C/C_0 in panel b is different than in panel a. Relevant experimental conditions are as follows: approach velocity = 0.021 cm/s, porosity = 0.43, mean grain diameter = 205 μm , and pH = 5.6–5.8. For clarity, every 10th data point is plotted in panel a and every point in panel b.

Table 3. Fraction of Deposited Bacterial Cells Eluted from the Column Following Release Experiments with a Low Ionic Strength Solution^a

strain	ionic strength (M)	fraction eluted ^b
D21g	$10^{-2.0}$	0.42 ± 0.1 ($n = 2$)
D21g	$10^{-1.5}$	0.68 ± 0.2 ($n = 4$)
D21g	$10^{-1.0}$	0.71 ± 0.3 ($n = 2$)
D21g	$10^{-0.5}$	0.54 ($n = 1$)
D21f2g	$10^{-1.5}$	0.72 ($n = 1$)
D21f2g	$10^{-0.5}$	0.49 ± 0.1 ($n = 2$)
JM109g	$10^{-1.0}$	0.57 ($n = 1$)

^a Low ionic strength solution was 10^{-4} M KCl. ^b n is the number of release runs for each cell and ionic strength condition.

solution and the amount of cells released in the elution pulse can be calculated by numerically integrating the breakthrough curve. From such calculations, the fraction of adhered cells eluted by the reduction in solution ionic strength can be determined.

Table 3 summarizes the amount of bacterial cells eluted from release experiments with the three strains. Release experiments were not conducted for deposition runs at ionic strengths lower than 10^{-2} M due to the minor amount of bacterial retention. As illustrated in Table 3, a significant fraction of the deposited bacteria were eluted from the column after the introduction of the low ionic strength solution, ranging from 0.42 to 0.72. This implies that the bacteria were not irreversibly attached to the quartz grain in a primary minimum, but rather that a substantial portion of the initially deposited cells were held reversibly in secondary energy minima. No clear trend was found for the amount released as a function of ionic strength or bacterial strain type.

In all repulsive electrostatic conditions examined, there was significant release of deposited cells, although always less than 100% of the originally deposited amount. This observation may indicate that a small fraction of the cells were most likely attached in primary minima. Such primary minimum deposition can be attributed to local charge (chemical) heterogeneities on the bacterial cells.^{43,55}

3.5.2. Deposition Behavior in the RSPF System. There is general agreement between the deposition

behaviors for the three *E. coli* strains evaluated in our two deposition systems. Both experimental techniques revealed that the deposition rates for JM109g were the greatest, followed by D21f2g and D21g. To quantitatively compare the deposition behaviors and the mechanisms involved, the dimensionless attachment (collision) efficiency was calculated for each system. The attachment efficiency is determined by normalizing the deposition rate at a given ionic strength by the deposition rate under “favorable” electrostatic conditions. Note that the attachment efficiency is the inverse of the stability ratio, W , commonly used in coagulation studies. Thus, the attachment efficiencies for the packed bed, α_{col} , and the RSPF system, α_{RSPF} , are

$$\alpha_{\text{col}} = \frac{k_d}{k_{d,\text{fav}}} \quad (6)$$

$$\alpha_{\text{RSPF}} = \frac{k_{\text{RSPF}}}{k_{\text{RSPF},\text{fav}}} \quad (7)$$

Theoretical deposition rates under favorable, transport-limited conditions cannot be calculated accurately due to the nonspherical shape of the bacteria and the irregular geometry of the quartz grains. Therefore, values for the favorable deposition rate in the column ($k_{d,\text{fav}}$) and the RSPF system ($k_{\text{RSPF},\text{fav}}$) were determined experimentally for each cell type. Favorable, nonrepulsive conditions were achieved in the column by use of quartz grains modified with aminosilane, which imparts a net positive ζ potential. The average $k_{d,\text{fav}}$ values for the D21g and D21f2g strains were virtually identical ($3.5 \times 10^{-2} \text{ s}^{-1}$), while the average $k_{d,\text{fav}}$ for JM109g was $6.4 \times 10^{-2} \text{ s}^{-1}$. Similarly, for the RSPF system, favorable (nonrepulsive) electrostatic conditions were created by use of aminosilane-modified coverslips. The resulting average favorable transfer rate coefficients ($k_{\text{RSPF},\text{fav}}$) for D21g, D21f2g, and JM109g were 0.245, 0.104, and 0.268 $\mu\text{m/s}$, respectively. The resulting attachment efficiencies α_{col} and α_{RSPF} calculated from eqs

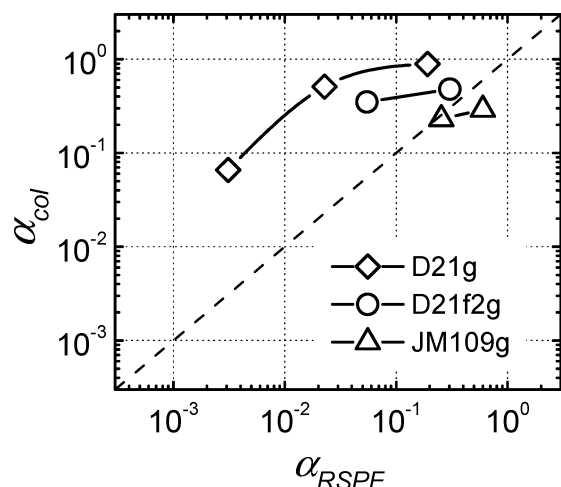


Figure 9. Comparison of α_{col} with α_{RSPF} for the three bacterial strains. The dashed diagonal line has a slope of unity.

6 and 7 are sensitive to the favorable deposition rates ($k_{\text{d,fav}}$ and $k_{\text{RSPF,fav}}$) as evident in the values reported in Table 1.

The attachment efficiencies for the column and RSPF deposition systems are compared in Figure 9 by plotting α_{col} versus α_{RSPF} . The dashed line indicates a slope of unity, on which experimental data points would lie if the adhesion efficiencies in the two systems were identical. The majority of the data points lie above the dashed line, not only indicating differences in the attachment efficiency between the two deposition systems but also implying different deposition mechanisms. We suggest this deviation arises from deposition occurring in the primary minimum in the RSPF system compared to deposition in both secondary and primary minima in the packed column. As we propose below, the hydrodynamics in the RSPF system do not allow for quantification of cells captured in secondary minima, leaving only cells deposited in a primary minimum to be enumerated.

The hydrodynamics in the two experimental deposition systems are different and so are the bacterial capture mechanisms. Bacterial cells held in a secondary minimum on a collector grain in the packed-bed column are subject to hydrodynamic forces that transport the cell along the quartz grain surface to the rear stagnation point (for a smooth spherical or near-spherical grain)^{55,59} or to other stagnant flow regions on the collector created by physical irregularities of the quartz grains.⁵⁵ Regardless of the actual location where the cell is captured on the quartz grain, it remains in the column and thus is accounted for when bacterial removal and the corresponding deposition rate are determined. In contrast, bacteria loosely held in secondary energy minima in the RSPF system are swept away by the radial component of flow parallel to the collector surface.^{55,60} Only cells deposited in primary minima will be retained in the RSPF field of view and enumerated for determination of the bacterial deposition rate.

Figure 9 clearly shows that the attachment efficiencies for D21g and D21f2g lie above the dashed line, indicating $\alpha_{\text{col}} > \alpha_{\text{RSPF}}$. The very large energy barriers and the relatively deep secondary minima (Figure 6 and Table 2) result in the capture of bacterial cells in the packed column predominantly in the secondary minimum. However, under these conditions, far fewer cells are captured in the

RSPF system, because quantifiable deposition of D21g and D21f2g occurs only in primary minima. It must be noted that D21f2g does approach the dashed line to a greater extent than D21g. This suggests greater deposition of D21f2g in primary minima than D21g, which may be attributable to heterogeneities on the cell surface—most likely due to membrane-bound proteins—that reduce electrostatic repulsion with the quartz because of the extremely short LPS molecule. The role of membrane-bound proteins will be elaborated on later in this paper.

The attachment efficiencies for JM109g lie along the dashed line (Figure 9). This observation may suggest that either the extent of primary and secondary minimum deposition of JM109g is similar in the two systems or the mechanism controlling JM109g adhesion involves interactions not accounted for in classical DLVO theory. As discussed earlier, the former explanation is unlikely since the RSPF system does not allow capture of bacterial cells in secondary energy minima. Efforts to correlate JM109g deposition behavior with DLVO interaction via the N_{DLVO} parameter (Figure 7), were unsuccessful, further suggesting that non-DLVO interactions are important for JM109g adhesion. Such interactions may originate from the presence of the relatively long O-antigen in the LPS of the JM109g. Initially, the JM109g may be slowly translating in a secondary minimum along the quartz surface, but while in close proximity to the collector the lengthy sugar chain will interact directly with the collector surface by non-DLVO, specific chemical interactions. Our earlier calculations (Table 2) indicate that, at the ionic strengths used in the RSPF system, the secondary minimum is located at distances much closer to the quartz surface than the length of the O-antigen, which can extend up to 30 nm from the surface.²⁹ This would permit the uncharged O-antigen to reach across the energy barrier and adsorb to the collector surface by specific interactions, such as hydrogen bonding.⁶¹ Similar interactions are not likely for D21g or D21f2g because the length of the LPS molecule on these strains is much smaller, on the order of only a few nanometers.

Additional support to the above arguments is the absence of measurable bacterial deposition for all three strains at moderate (10^{-2} M) and lower ionic strengths in the RSPF system (Figure 5). Under these ionic strength conditions, however, significant deposition was observed in the packed column experiments (Figure 4). At the lower ionic strengths, charge heterogeneities play a less important role,⁶² and the large electrostatic repulsive barriers hinder deposition in primary minima in the RSPF system. Furthermore, at lower ionic strengths, the location of the secondary minima is farther from the surface (Table 2), which may prevent the O-antigen of JM109g from interacting with the quartz surface and resulting in significant deposition.

3.6. Bacterial Adhesion Dependence on Cell Surface Polymers. Having discussed the electrostatic, van der Waals, and hydrodynamic influences on cell adhesion, the relative role of bacterial surface polymers is now further addressed. Bacterial surface polymer interactions have been noted as contributing to cellular adhesion.^{14,63} Hence, the following polymers are considered: extracellular polymeric substances (EPS), lipopolysaccharides (LPS), and membrane-bound proteins.

(61) Jucker, B. A.; Harms, H.; Hug, S. J.; Zehnder, A. J. B. *Colloid Surf. B—Biointerfaces* **1997**, *9*, 331.

(62) Song, L. F.; Johnson, P. R.; Elimelech, M. *Environ. Sci. Technol.* **1994**, *28*, 1164.

(63) Razatos, A.; Ong, Y. L.; Sharma, M. M.; Georgiou, G. *Proc. Natl. Acad. Sci. U.S.A.* **1998**, *95*, 11059.

(59) Spielman, L. A. *Annu. Rev. Fluid Mech.* **1977**, *9*, 297.

(60) Adamczyk, Z.; Siwek, B.; Warszynski, P.; Musial, E. *J. Colloid Interface Sci.* **2001**, *242*, 14.

3.6.1. EPS. The development of a conditioning layer (film) and the strengthening of attachment in early stages of biofilm formation have been attributed to bacterial EPS.^{13,64} The *E. coli* K12 used in this study has been reported as producing little or no EPS.⁶³ Other K12 strains have been noted as producing EPS,^{65,66} but these mutant forms are not used in this investigation. Therefore, since it is doubtful that over the time course of our experimentation the planktonic bacteria would form EPS, we do not attribute the adhesion behavior to EPS.

3.6.2. LPS. Selection of the three *E. coli* K12 strains allowed us to investigate the relative role of the LPS molecule presence and composition in cell adhesion. The actual steric orientation and length of the LPS molecule for these three strains is not known, although the relative length has been surmised by such techniques as X-ray diffraction, molecular dynamics simulations, and analysis of the sugar content.^{26,28,47} Our adhesion experiments were able to resolve the subtle differences in deposition rates (both k_d and k_{RSPF}) between the strains yet demonstrated there is no direct relationship between the LPS length and deposition rate. The one trend observed consistently was that the strain with the longest LPS, JM109g, resulted in the greatest deposition rate of the three strains in both experimental systems.

We attribute the adhesion behavior of JM109g to chemical interactions, not otherwise included in classic DLVO theory, for which supporting evidence can be found in the literature.^{28,67} Previous work utilizing molecular modeling theorized that the conformation of the LPS is “bent” such that the O-antigen region of the polymer covers, or lies over, other adjacent surface-bound molecules.²⁸ It is possible that the O-antigen on the JM109g is in the “bent” conformation and is the dominant portion of the LPS interacting with the surrounding medium and collector surface. Thus, the O-antigen could “shield” charged functional groups, which would otherwise influence electrostatic double-layer interactions. This hypothesis is consistent with our measurements of JM109g having the least negative ζ potential of the three strains.

Another possible contributing factor may be “roughness” of the JM109g outer membrane surface. AFM analysis of this particular strain revealed clumps or patches of 600–3500 LPS molecules.²³ This study further reported molecular simulations of the O-antigen assembly and found approximately 50% of the O-antigens have only 0–3 repeating units, while the remaining have up to 26 repeating units. Roughness caused by clumps of lengthy O-antigens and regions of truncated LPS molecules²³ will result in a distribution of interaction energies between the bacterial cell and a collector surface, and a reduction in the resulting net (average) repulsive interaction energy.⁶⁸ The lower overall energy barrier to deposition of the JM109g due to local cell surface roughness, which is not accounted for in classical DLVO theory, supports the observation that this strain deposits to a greater extent than the other strains.

Deviation of JM109g from the adhesion behavior of D21g and D21f2g could also be due to this cell originating from a different parent strain of *E. coli* K12. The JM109g diverges from the interrelated mutants D21g and D21f2g

based on mutations in the original nonpathogenic *E. coli* K12.^{33,47} D21 was first isolated from the K12 strain on the basis of its ampicillin resistance and no apparent defect in LPS.^{33,47} The D21f2 arose from a series of two spontaneous mutations forming an ampicillin-resistant and severely truncated LPS-producing mutant.^{34,47} The D21 mutant series has been noted as having a reduced amount of major membrane protein B.⁴⁷ This slight difference in protein presence and LPS structure is a direct result of the mutants being from different parent strains and may partially explain the variation in their observed deposition behaviors.

3.6.3. Membrane-Bound Proteins. The influence of membrane-bound proteins on bacterial adhesion is still not fully understood. Exposed membrane-bound proteins would contribute to the electrostatic interactions between the bacterium and the quartz. The degree of protein exposure is dependent on the composition of the LPS: for instance, the presence of an O-antigen is likely to hide the proteins.^{28,61} The strain with the most truncated form of the LPS, D21f2g, demonstrated greater adhesion efficiency than the D21g in both experimental systems. This behavior may be attributed to the core polysaccharide portion of D21g shielding some of the charges originating from proteins, whereas the proteins on the D21f2g are exposed and can contribute to the electrostatic interactions.⁴³ As discussed earlier in the paper, proteins can produce local charge heterogeneities and, hence, lower electrostatic repulsion because of the inherent distribution of charged functional groups on the protein.

4. Conclusion

The two experimental techniques employed, a packed-bed column and a radial stagnation point flow (RSPF) system, allowed for a thorough investigation of bacterial adhesion kinetics and provided useful insights into the role of LPS. The importance of the distribution of charged functional groups on the LPS and the outer membrane of the bacteria was investigated by utilizing three *E. coli* K12 strains with well-characterized LPS molecules. For the strains with significant exposed charged groups, adhesion is dominated by electrostatic interactions, in qualitative agreement with classic DLVO theory. However, for the bacterial strain with the full LPS molecule, the uncharged O-antigen portion of the LPS shields charged functional groups, which results in significantly reduced electrostatic interactions. The O-antigen may also be able to reach across the energy barrier and interact directly with collector surfaces by non-DLVO interactions.

Further insight into bacterial deposition kinetics can be gained by considering the role of the fluid flow field and hydrodynamic forces. The hydrodynamics in the two deposition systems are distinct and therefore capture different adhesion mechanisms, as indicated by the notable disparity in the corresponding attachment efficiencies. We propose this deviation is due to the hydrodynamics of the RSPF system not allowing for cells present in a secondary minimum to deposit, thus enumerating only cells deposited in a primary minimum. On the other hand, cells in the packed column system deposit in both secondary and primary minima, resulting in higher attachment efficiencies than in the RSPF system.

Acknowledgment. We acknowledge the National Science Foundation, Collaborative Research Activities in Environmental Molecular Sciences (Grant CHE-0089156), the National Water Research Institute, the Yale Institute for Biospheric Studies, and Professor H. P. Spaink (Leiden University, The Netherlands) for use of the EGFP plasmid.

(64) Olofsson, A. C.; Hermansson, M.; Elwing, H. *Appl. Environ. Microbiol.* **2003**, *69*, 4814.

(65) Ryu, J. H.; Beuchat, L. R. *J. Appl. Microbiol.* **2003**, *95*, 1304.

(66) Graham, L. L.; Harris, R.; Villiger, W.; Beveridge, T. J. *J. Bacteriol.* **1991**, *173*, 1623.

(67) Jucker, B. A.; Zehnder, A. J. B.; Harms, H. *Environ. Sci. Technol.* **1998**, *32*, 2909.

(68) Bhattacharjee, S.; Ko, C. H.; Elimelech, M. *Langmuir* **1998**, *14*, 3365.